Proceedings of the ASME 27th International Conference on Offshore Mechanics and Arctic Engineering
OMAE2008
June 15-20, 2008, Estoril, Portugal

OMAE2008-57803

SPATIAL VARIATION OF DRAG ON LONG CYLINDERS IN SHEARED FLOW

Vikas Jhingran
Department of Mechanical Engineering
Massachusetts Institute of Technology

Vivek Jaiswal
Department of Mechanical Engineering
Massachusetts Institute of Technology

J. Kim Vandiver
Department of Mechanical Engineering
Massachusetts Institute of Technology

ABSTRACT

A method is described for measuring the local drag coefficient on a long cylinder which exhibits vortex-induced vibration (VIV). Results are shown from a field experiment in which a long flexible pipe was instrumented with two-hundred and eighty fiber optic strain gauges. The measured local drag coefficients are compared to a commonly used drag coefficient prediction formula. The formula is shown to be useful as a tool for predicting the average drag coefficients for the whole cylinder but is not able to accurately capture local variation in C_D. The local C_D measurements also reveal the location of VIV source regions.

INTRODUCTION

Amplification of drag forces due to Vortex-Induced Vibration (VIV) has been studied for many years. Formulations for the amplifications were developed by Vandiver and others in the late 1970's and early 1980's. Recent laboratory experiments on a rigid cylinder undergoing VIV by Jauvtis & Williamson [2] indicate great variations in the drag amplification factor when reduced velocity is varied.

Spatial variations in local reduced velocities are common in realistic ocean current environments where flexible cylinders are placed in sheared currents. However, the local drag amplification factors corresponding to the local reduced velocities have never been reported primarily due to the difficulty in measuring local drag forces in field experiments. In this paper, the authors, using strain data from field experiments performed off the coast of Miami in the Gulf Stream, present an approach to estimate the local mean drag coefficient

Numerous researchers studying VIV have found that the drag forces are amplified when a flexible cylinder is placed in a current and it undergoes VIV. A large volume of research has been performed to develop methods for predicting drag coefficient amplification factor in the presence of VIV. This amplification factor is used to multiply the drag coefficient of a stationary rigid cylinder in fluid flow to yield a prediction of the drag coefficient for the vibrating cylinder.

Several formulations have been derived for the amplification factor using both field experiments [4] and laboratory tests [1]. The most commonly used formulation in the oil and gas industry has been proposed by Vandiver [4] and is shown in Equation (1.1). An example of the amplification can be obtained by assuming a root mean square (RMS) amplitude to diameter ratio, $(y_{rms}(z)/D)$, value of 0.707, equivalent to a peak amplitude to diameter ratio of 1.0. Such amplitudes are commonly seen in lightly damped pipes undergoing VIV, as is common in the oil and gas industry. The amplification factor from Equation 1.1 is thus found to be 2.31, implying a greater than doubling of the drag forces due to VIV.

$$C_D(z) = C_{Do} * C_{D,amp}(z)$$
$$C_{D,amp} = 1 + 1.043 * (2y_{rms}/D)^{0.65} \qquad (1.1)$$

$C_D(z)$ = Local Drag Coefficient

$C_{D,amp}(z)$ = Drag Amplification

C_{Do} = Drag Coefficient of a stationary cylinder

$y_{rms}(z)$ = Local RMS Amplitude of vibration

D = Diameter of pipe

Most of the work related to drag amplification has been based on experiments performed with rigid cylinders or short flexible cylinders responding in a standing wave pattern. To the knowledge of the authors, the more realistic problem of drag amplification for structures in sheared flows, which respond with traveling waves, has not been studied. Also, the C_D values that have been reported earlier for flexible cylinders have been based on the total drag force experienced by the structure. No attempt has been made to study the spatial variation of drag forces along the length of the structure.

Two field experiments, sponsored by DEEPSTAR, were conducted in the Gulf Stream. In the second experiment, a 500.4-foot-long and 1.43 inch outer diameter pipe with embedded fiber optic strain gauges was towed in sheared currents. Strain measurements were recorded at 70 locations at 7 ft regular intervals along the length of the pipe. It was possible to estimate the local drag force per unit length and the vibration amplitude from the strain measurements. In the following sections, a brief description of the experiments and the methods for estimation of the local drag force and vibration amplitude is presented.

EXPERIMENT DESCRIPTION

The second DEEPSTAR sponsored Gulf Stream Experiment was conducted in October 2006. The set-up for the experiment is shown in Figure 1.

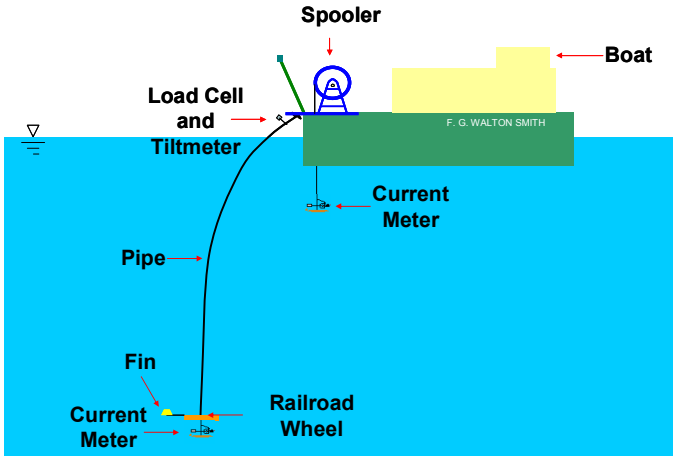

Figure 1. Set-up for the Gulf Stream Experiments 2006.

The experiment was conducted on the Research Vessel F. G. Walton Smith from the University of Miami using a fiber glass composite pipe 500.4-feet-long(152.4 m) and 1.43 inches(3.63 cm) in outer diameter. A railroad wheel weighing 805 lbs (dry weight, 725 lbs in water(3225 N)), was attached to the bottom of the pipe to provide tension.

Strain gauges were used to measure the VIV response of the pipe. Eight optical fibers containing thirty five strain gauges each were embedded in the outer layer of the composite pipe. The gauges had a resolution of 1 micro-strain.

The strain gauges in each fiber were spaced 14 feet(4.267 m) apart and the two fibers in the same quadrant were placed such that their strain gauges were offset by 7 feet(2.133m). This arrangement is shown in Figure 2.

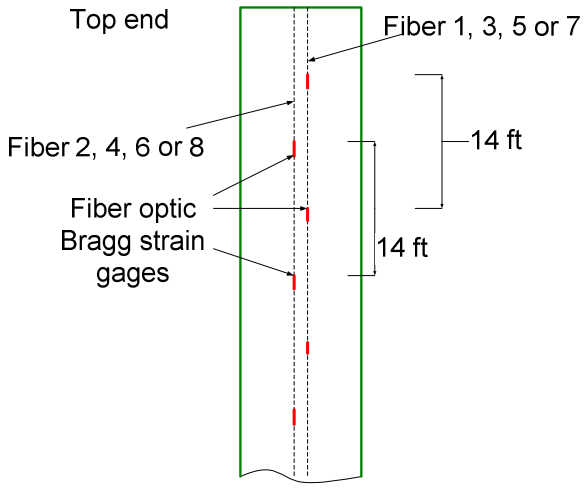

Figure 2. Arrangement of strain gauges in a quadrant.

Two fibers were located in each of the four quadrants of the pipe, as seen in Figure 3**.** It should be noted that during the experiments, the quadrants were not necessarily aligned with the cross-flow (CF) or in-line (IL) directions. As a result, the gauges in all the quadrants would typically reveal components of both CF and IL vibrations. The total CF strain component can however be computed by making use of data from an orthogonal pair of gauges. The method to do this will be shown later in the paper.

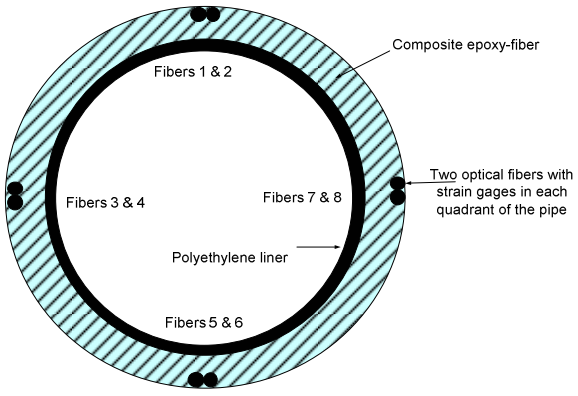

Figure 3. Cross-Section of the Pipe from the Gulf Stream Test.

The R/V F. G. Walton Smith is equipped with Acoustic Doppler Current Profilers (ADCP). During the experiments, the ADCP was used to record the current velocity and direction in the depth of the water column. Additional instrumentation included a tilt meter to measure the inclination at the top of the pipe, a load cell to measure the tension at the top of the pipe, a pressure gauge to measure the depth of the railroad wheel and two mechanical current meters to measure current at the top and the bottom of the pipe.

The pipe properties are listed in Table 1.

Table 1. Gulf Stream Experiment 2006 pipe properties

Inner Diameter	0.98 in(0.0249 m)
Outer Diameter	1.43 in(0.0363 m)
Optical Fiber Diameter	1.37 in(0.0330 m)
EI	2.14×10^5 lb in^2 (613 Nm^2)
Modulus of Elasticity (E)	1.33×10^6 lb/in^2 (9.21e9 N/m^2)
EA	7.47×10^5 lb (3.32e6 N)
Weight in Seawater	0.133 lb/ft (flooded in Seawater) (1.942 N/m)
Weight in air, w/trapped water	0.511 lb/ft (7.46 N/m)
Effective Tension at the bottom end	725 lb, submerged bottom weight (3225N)
Material	Glass fiber reinforced epoxy
Length	500.4 ft (152.4 m) (U-joint to U-joint)

A COMPARISON OF MEASURED AND PREDICTED LOCAL DRAG COEFFICIENT

Equation 1.1 is a commonly used C_D prediction formulation. It is normally used in conjunction with a VIV response prediction program such as SHEAR7. It requires as input predicted or measured values of local VIV response amplitude expressed as a local amplitude-to-diameter ratio. One does not normally have access to measured local response when predicting values of C_D. However, in this paper the authors are able to make a direct assessment of the accuracy of Equation 1.1 by using measured local *A/D* values as inputs and predicted C_D values as outputs. The prediction is then compared directly to the measured C_D values. In the next section the method for obtaining the measured *A/D* values is described. Then the method for obtaining the measured C_D values is presented. In the Results section the measured values are compared to the predictions.

Drag Coefficient Prediction Based on Dynamic Response Amplitude

Since the measured response of the pipe is strain, it is not possible to get the CF displacement amplitude from it directly. However, it can be estimated, if it is assumed that the waves in the pipe are sinusoidal traveling waves. This means that the CF displacement at any time *t* and at any given location *z* can be written as:

$$y(z,t) = A\sin(\omega t - kz + \alpha) \tag{1.2}$$

and the curvature is given by:

$$y_{zz}(z,t) = -Ak^2\sin(\omega t - kz + \alpha) \tag{1.3}$$

The relationship between the bending strain and the curvature is:

$$\varepsilon(z,t)_{bending} = -ry_{zz}(z,t) \tag{1.4}$$

where *r* is the distance from the neutral axis to the point where the strain is measured. Using Equations (1.2), (1.3) and (1.4), the RMS CF displacement and strain are related as follows:

$$y_{rms} = \frac{\varepsilon_{rms}}{rk^2} \tag{1.5}$$

The wavenumber (k) can be estimated from the estimated phase speed. For the waves in the pipe, the wavenumber can be written as:

$$k = \frac{\omega}{c_s(\omega)} \tag{1.6}$$

One of the ways to estimate the phase speed of the various frequency components in a wave is to compute the change in their phase as they travel from one point to another along the pipe. In order to compute the phase of the frequencies in a signal, the Fourier Transform of the signal is computed. The Fourier Transform of the signal is a set of complex numbers, each corresponding to a discrete frequency component of the signal. The arguments of these complex numbers represent the phase (φ) of the corresponding frequency component and the magnitude represents the amplitude. If the signals are measured by two sensors which are located at points z_1 and z_2 and the phases ($\varphi_1(\omega)$ and $\varphi_2(\omega)$) of these signals, which are functions of frequency, are computed, then the rate of change in phase is given by:

$$\frac{\Delta\varphi}{\Delta z} = \frac{\varphi_2 - \varphi_1}{z_2 - z_1} \tag{1.7}$$

The phase speed is then given by:

$$c_s(\omega) = \frac{\omega}{\Delta\varphi/\Delta z} \tag{1.8}$$

where ω is in rad/s. Phase speed estimates for discrete frequencies in the band 0.9 to 1.1 times the primary CF response frequency (1x frequency, defined in the last paragraph of this section) are computed. The mean value of these phase speed estimates is taken as the phase speed of the 1x frequency component.

The machinery to estimate the RMS response amplitude from the measured RMS strain data is now in place. However, before making further progress, the problem mentioned earlier – the lack of measured CF strain at any given location due to the non-alignment of the orthogonal pair of strain gauges with the CF and IL directions (see Figure 4) – must be addressed. The fact that the gauges were not

aligned with the CF and IL directions becomes evident from the PSD of strain at a given location as shown in Figure 5.

To estimate the CF RMS strain, the fact that the square root of the area under a power spectral density (PSD) curve is the RMS value of the time series used to compute the PSD is used. A pair of orthogonal gauges is chosen at a location and the PSD of the signal measured by each of them is computed. The two PSDs are added to get a combined PSD (see Figure 6).

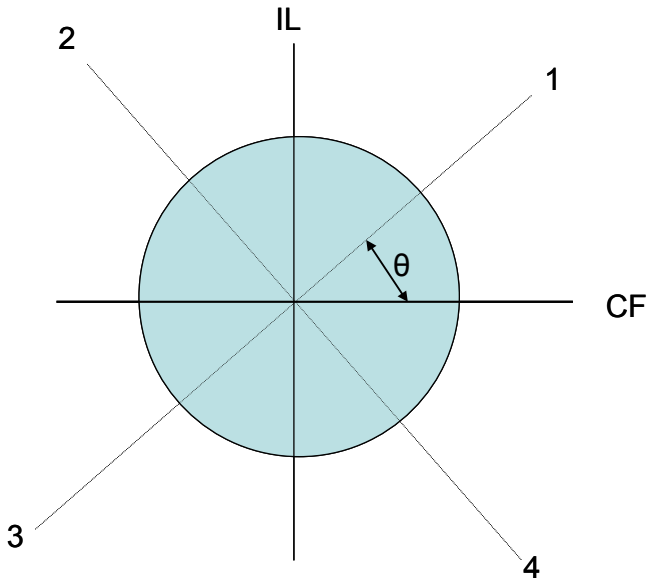

Figure 4. The quadrants may not necessarily be aligned with the CF and IL directions.

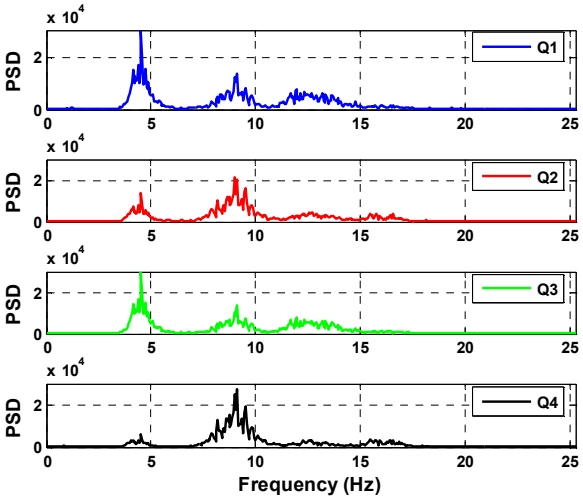

Figure 5. Power Spectral Density (PSD) of strain at axial location z/L = 0.42 (z/L = 0 is at the bottom end of the pipe). PSD in all the four quadrants is shown. Both IL and CF vibration frequency content can be seen in all the quadrants. (Test case identifier 20061022153003)

Equations (1.9) through (1.13) show that adding the PSDs of orthogonal gauges is equivalent to adding the PSDs of CF and IL directions.

$$\varepsilon_1 = \varepsilon_{CF}\cos\theta + \varepsilon_{IL}\sin\theta \quad (1.9)$$

$$\varepsilon_2 = -\varepsilon_{CF}\sin\theta + \varepsilon_{IL}\cos\theta \quad (1.10)$$

$$\Phi_1 = \Phi_{CF}\cos^2\theta + \Phi_{IL}\sin^2\theta \quad (1.11)$$

$$\Phi_2 = \Phi_{CF}\sin^2\theta + \Phi_{IL}\cos^2\theta \quad (1.12)$$

$$\Phi_{Total} = \Phi_1 + \Phi_2 = \Phi_{CF} + \Phi_{IL} \quad (1.13)$$

where ε represents the strain, Φ represents the PSD of the strain and the subscripts refer to the directions in which each of quantities are measured.

In the next step, the primary CF response frequency (1x frequency) is determined. The 1x frequency is defined as the frequency corresponding to the first peak in the combined PSD (see Figure 6). Finally, the area under the combined PSD curve for frequency values ranging from 0.5 to 1.5 times the 1x frequency is computed. The square root of this area under the combined PSD is then taken as the estimate for RMS CF strain. Depending upon the number of working strain gauges at any given location, it is possible to get CF strain estimates from up to four orthogonal sensor pairs. Equation (1.5) may then be used to estimate the 1x displacement from the 1x RMS strain. Having obtained the response amplitude, the local drag amplification and drag coefficient can be estimated using Equation(1.1).

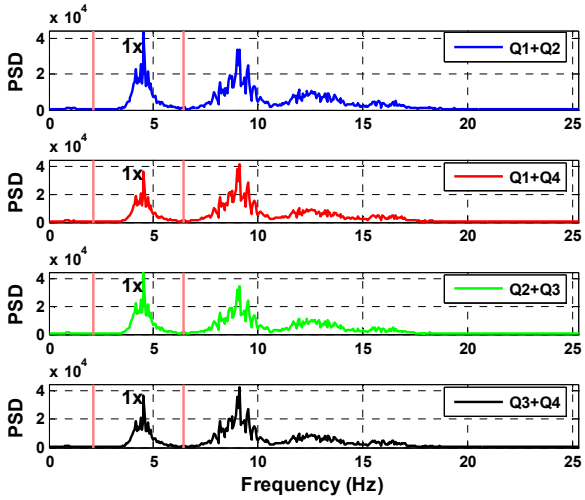

Figure 6. Sum of the PSD of orthogonal pairs of gauges at axial location z/L = 0.42 (z/L = 0 is at the bottom end of the pipe). All four possible pairs have been shown. Also shown in the plots are the 1x frequency peaks and the 0.5 to 1.5 times 1x frequency band. (Test case identifier 20061022153003)

Drag Coefficient Estimation Based on Measured Static Bending Strain

The equation of motion for a pipe undergoing VIV can be written as:

$$(m(z)+m_a(z,w))\frac{\partial^2 y}{\partial t^2}+c(z)\frac{\partial y}{\partial t}+(EI(z)\frac{\partial^4 y}{\partial z^4}-T(z)\frac{\partial^2 y}{\partial z^2})=F(z,t) \quad (1.14)$$

where

$m(z)$ = local mass per unit length
$m_a(z)$ = local added mass per unit length
$c(z)$ = local damping coefficient
$EI(z)$ = local bending stiffness
$T(z)$ = local Tension
$F(z,t)$ = local forcing in phase with velocity

Taking a temporal mean of the terms in the above equation, the acceleration and velocity terms vanish because they are zero-mean oscillatory processes. Further, for a tension dominated beam undergoing VIV, as was the case in the Miami experiments, the term corresponding to EI can also be dropped. This reduces Equation (1.14) to

$$-T(z)\overline{y_{zz}{}^t}=\overline{F(z)^t} \quad (1.15)$$

where the temporal averaged inline force $\overline{F(z)^t}$ is the local mean drag force per unit length and derivatives with respect to z are denoted using subscripts.

As the Gulf Stream experiments measured strain, equation (1.15) can be rewritten using Equation (1.4) and the quantities measured during the Gulf Stream experiments, as shown in Equation (1.16)

$$-T(z).\overline{\varepsilon(z)^t}.\frac{2}{D_{op}}=\overline{F(z)^t} \quad (1.16)$$

where

$$\varepsilon=\frac{D_{op}/2}{R};$$

$\varepsilon=\text{Strain}\quad D_{op}=\text{Optical Diameter of Pipe}$

$R=\text{Radius of curvature}$

$R=\frac{1}{\sigma};\quad \sigma=\text{curvature}$

$F=T\times\sigma;\quad T=\text{Tension}$

The drag force per unit length can be written using a drag coefficient as

$$C_D(z)=F(z)/\tfrac{1}{2}\rho DV(z)^2 \quad (1.17)$$

where $V(z)$ is the local current speed and D is the pipe outer diameter. Using (1.16) $C_D(z)$ can be expressed as:

$$C_D(z)=\frac{4T(z)\overline{\varepsilon(z)^t}}{\rho DD_{op}V(z)^2} \quad (1.18)$$

In order to illustrate the effectiveness of this method, C_D estimates for an experiment with fairings are shown in Figure 7. The figure also shows the normal incident current for the case considered. In this case, the bottom 40% of the pipe (z/L = 0 to 0.4) was covered with fairings and the top 60% (z/L = 0.4 to 1.0) was bare pipe. The fairings suppress VIV and have lower drag coefficients than the bare pipe. In the region with fairings, the average C_D was approximately 0.7 and in the bare region the average C_D was 2.3. The C_D values obtained for the fairings are in good agreement with measurements made by the manufacturer in tow tank experiments. Similar results were obtained from several test runs with fairings at a variety of speeds. Good agreement with independently measured fairing drag coefficients provided confidence in the method. The method was next applied to estimation of drag coefficients on a bare cylinder in sheared flow.

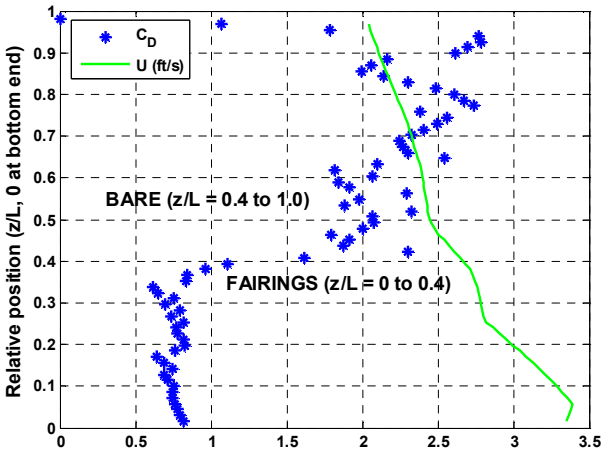

Figure 7. Normal incident current (ft/s) and drag coefficient estimates from mean static bending strain for a 40% fairing coverage case. (Test case identifier 20061020222947)

RESULTS

A number of important results are shown by means of two example cases: 20061023205043 and 20061022153003. The current profile, reduced velocity and the estimated RMS A/D response for the first case (20061023205043) are shown in Figure 8. The current profile is sheared and has a higher magnitude towards the bottom end of the pipe. The current speed in the figure is the component perpendicular to the pipe. The reduced velocity is based on the 1x response frequency determined from the PSD of strain. The region with $5 < V_r < 7$ is highlighted with red stars as the potential power-in region. The RMS A/D is highest for $.2 < z/L < .4$ and then decays going towards the top end.

RMS A/D estimates were obtained only in the range from $z/L = 0$ to $z/L = 0.65$ because there were no orthogonal strain gauge pairs with good data at higher z/L values.

The pipe is vertical at the bottom end and gradually tilts toward the vessel as one progresses up the pipe to the top end. At the higher speeds the angle the pipe made with the vertical could exceed 45 degrees at the highest test speeds. The velocity shown in the profiles is the normal incidence component of the flow speed. In the region toward the top of the pipe the low speed values coupled with strain signal noise, resulted in rather large confidence bounds on the estimated drag coefficient values. This is reported in the appendix. Many strain gauge data points are missing near the top of the pipe, because the total static plus dynamic strain exceeded the dynamic range of the decoding electronics. Fortunately the VIV power-in regions were located in the lower parts of the test pipe where the velocities were higher. Throughout this paper, the strain and drag coefficient results near the top of the pipe should be disregarded due to the large uncertainty.

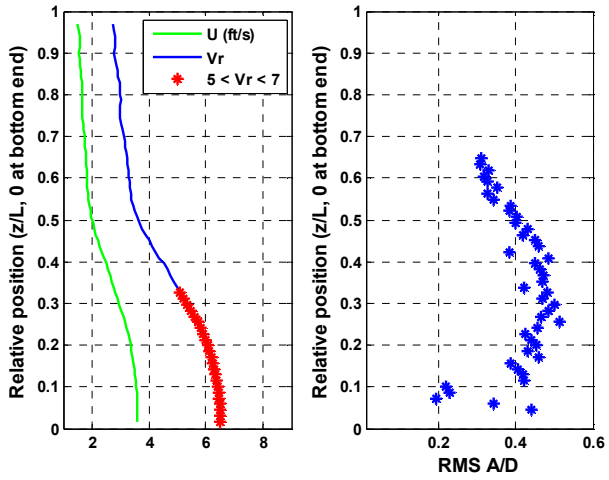

Figure 8. Normal incident current (ft/s), Reduced Velocity based on 1x response frequency and the estimated RMS A/D for case 20061023205043.

As noted in Marcollo et al. [3], the response of the pipe during the Gulf Stream experiments showed traveling wave behavior. Figure 9 shows the band pass filtered, measured time series at different locations. The filtering was performed to include frequency components in the range of 0.5 to 1.5 times the 1x frequency. Following a constant phase (say the crest, as shown by the arrows in the figure), one can see the waves traveling from the bottom end towards the top end. There is a small region close to the bottom end ($z/L = 0.0$ to 0.1) where the behavior is a mix of standing and traveling waves.

Figure 10 shows the measured static bending strain for the same case. It can be seen from the figure that the static bending strain and consequently the drag force is higher in the probable power-in region and drops off significantly outside this region. The authors therefore believe that the region of increased drag is a good indicator of the power-in region.

Figure 11 shows the measured and predicted local drag coefficient, using the methods described in the previous sections. The following points are evident from the figure:

- The C_D is under-predicted in the power-in region by the A/D based formula.
- The static strain based C_D measurement is able to capture abrupt changes in local drag. The A/D based C_D prediction is unable to do so because the variation in A/D is gradual.
- The peak in C_D based on static strain is not at the same location as the maximum A/D response.
- The maximum C_D value occurs in the region of traveling wave growth $(.1 < z/L < .3)$ and not in the standing wave region near the boundary or other regions of traveling wave response.

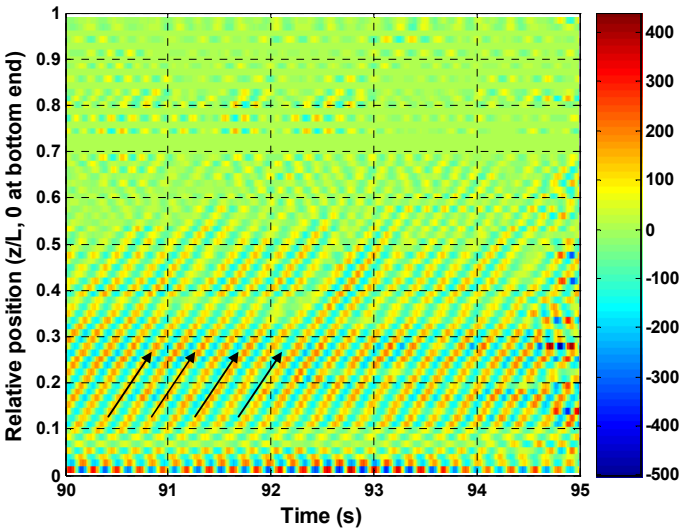

Figure 9. Time series plot of filtered strain (in micro strain) measured in quadrant 4 at different locations along the length of the pipe for case number 20061023205043. The waves can be seen traveling from bottom end towards the top end as indicated by the arrows.

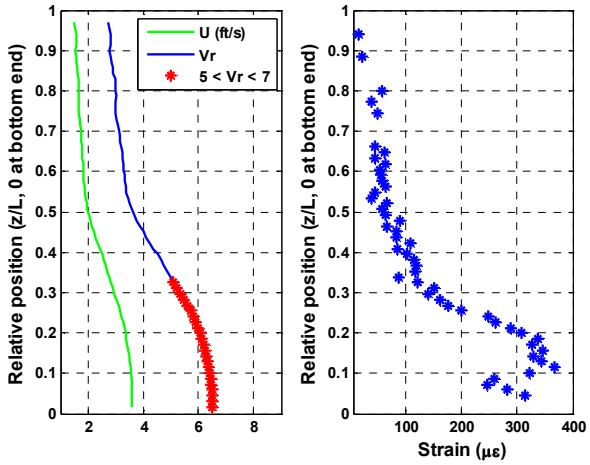

Figure 10. Normal incident current (ft/s), Reduced Velocity based on 1x response frequency and the static bending strain for case 20061023205043.

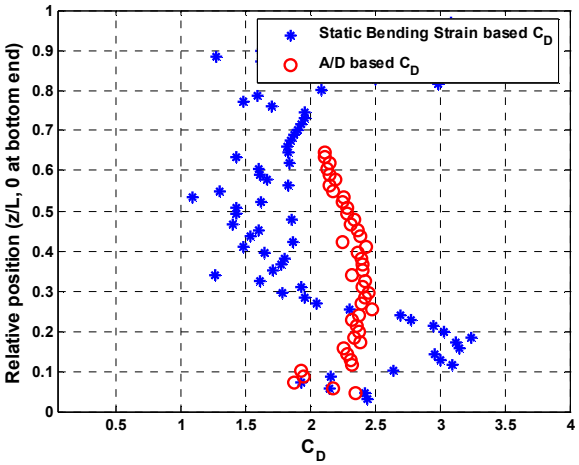

Figure 11. Measured drag coefficient based on Static Bending Strain and predicted drag coefficient based on measured RMS A/D for case 20061023205043.

Results from the second case (20061022153003) are now presented. The current profile, reduced velocity and the estimated RMS *A/D* response are shown in Figure 12. Unlike the previous case, this current profile has a peak away from the bottom end. The current decreases going towards both ends from the peak. Also note that the estimated response amplitude (*A/D*) shows two local peaks, one at $z/L = 0.20$ and the other at $z/L = 0.40$.

Based on an expected range of reduced velocity of $5 < V_r < 7$, the potential power-in region in this case extends from $z/L = 0.18$ to 0.42, and is indicated by red dots on the reduced velocity curve in Figure 12. Since the power-in region is located away from the bottom end, one can expect the waves to travel away from this region towards the top and bottom end. Indeed, the waves travel away from the power-in region as shown in Figure 13.

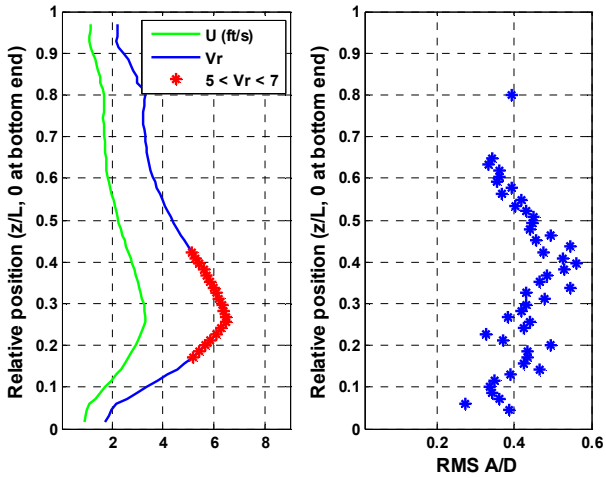

Figure 12. Normal incident current (ft/s), Reduced Velocity based on 1x response frequency and the estimated RMS *A/D* for case 20061022153003.

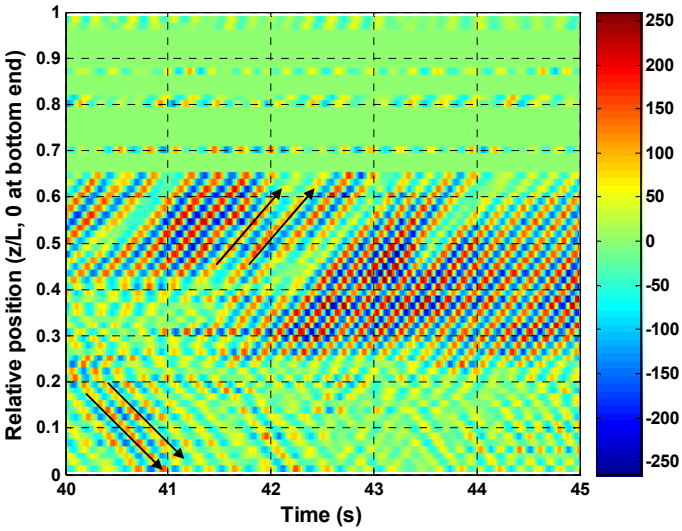

Figure 13. Time series plot of filtered strain (in micro strain) measured in quadrant 3 at different locations along the length of the pipe for case number 20061022153003. The waves can be seen traveling away from the power-in region towards the top and bottom end.

The static bending strain, shown in Figure 14, also shows two peaks. The peaks correspond to regions with high drag force. Both the peaks appear to be happening in regions where the response shows traveling wave growth.

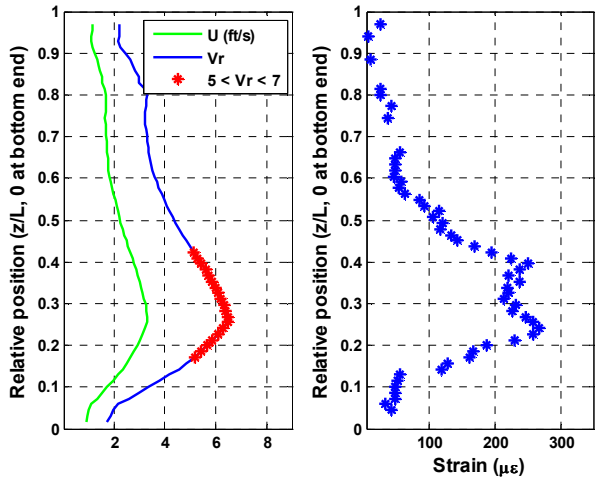

Figure 14. Normal incident current (ft/s), Reduced Velocity based on 1x response frequency and the static bending strain for case 20061022153003.

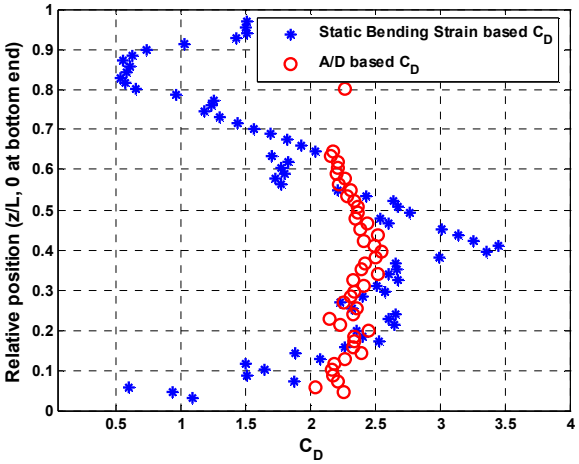

Figure 15. Measured drag coefficient based on Static Bending Strain and predicted drag coefficient based on measured RMS A/D for case 20061022153003

A comparison of the measured and predicted C_D values shows that the *A/D* based prediction formulation under-predicts the drag in the power-in region (see Figure 15).

CONCLUSIONS

A method of estimating local drag coefficient on a flexible pipe has been presented. The method is able to capture local variations in drag coefficient and is helpful in identifying the power-in region.

Further, the following may be concluded:

1. The estimated local drag coefficients show reduced velocity (V_r) dependence. It is observed that the drag is high in the region with $5 < V_r < 7$. Outside this band of V_r, the drag shows a rapid drop to lower drag coefficient values. The RMS displacement however does not show such a sudden drop because of the persistence of traveling waves. Drag coefficient prediction formulas based on A/D estimates will therefore fail to capture local variations in C_D.
2. The *A/D* based drag amplification formulation under-predicts the drag in the power-in region. The *A/D* based prediction formula does, however, provide a good estimate of mean drag averaged over the entire cylinder.
3. The maximum local drag coefficient is associated with regions of peak VIV excitation and may not coincide with the location of the maximum *A/D* response.

NOMENCLATURE

A	*Amplitude [length]*
C_D, C_{Do}	*Drag coefficient [non-dimensional]*
$C_{D,amp}$	*Drag amplification [non-dimensional]*
D	*Diameter [length]*
E	*Modulus of elasticity [mass length^{-1} time^{-2}]*
I	*Area moment of inertia [length^4]*
F	*Drag force per unit length [mass time^{-2}]*
L	*Pipe length [length]*
R	*Radius of curvature [length]*
T	*Tension [mass length time^{-2}]*
U, V	*Current speed [length time^{-1}]*
V_r	*Reduced velocity [non-dimensional]*
Φ	*Power spectral density of strain [time^{-1}]*
c	*Damping coefficient [mass length^{-1} time^{-1}]*
c_s	*Phase speed [length time^{-1}]*
k	*Wavenumber [length^{-1}]*
m	*Mass per unit length [mass length^{-1}]*
t	*Time [time]*
r	*Distance of optical fiber from neutral axis [length]*
y	*Displacement [length]*
z	*Axial distance along pipe [length]*
α	*Phase angle [non-dimensional]*
ε	*Strain [non-dimensional]*
θ	*Angle [non-dimensional]*
ρ	*Fluid density [mass length^{-3}]*
σ	*Curvature [length^{-1}]*
φ	*Phase [non-dimensional]*
ω	*Angular frequency [time^{-1}]*

ACKNOWLEDGMENTS

This research was sponsored by the DEEPSTAR Consortium, the Office of Naval Research Ocean Engineering and Marine Systems program (ONR 321OE) and the SHEAR7 JIP. The authors wish to thank the crew of the R/V F. G. Walton Smith at the University of Miami Rosenstiel School of Marine and Atmospheric Science. The authors also thank Jim Chitwood from Chevron, Robert Knapp from Insensys and Fiberspar. The authors would also like to thank

their research team members Dr. Susan Swithenbank and Dr. Hayden Marcollo.

REFERENCES

[1] Griffin, O. M. (1985). *Vortex-induced vibrations of marine cables and structures* No. 5600. Washington, D.C.: National Research Laboratory.

[2] Jauvtis, N., & Williamson, C. H. K. (2004). The effect of two degrees of freedom on vortex-induced vibration at low mass and damping. *Journal of Fluid Mechanics, 509*, 23.

[3] Marcollo, H., Chaurasia, H., & Vandiver, J. K. (2007). Phenomena observed in VIV bare riser field tests. *Proceedings of the 26th International Conference on Offshore Mechanics and Arctic Engineering, 26*

[4] Vandiver, J. K. (1983). Drag coefficients of long flexible cylinders. *Offshore Technology Conference – 4490.*

[5] Jhingran, V. (2008). Drag Amplification and Fatigue Damage in Vortex-Induced Vibration. PhD Thesis, Massachusetts Institute of Technology, Cambridge, MA.

APPENDIX

Error bounds on C_D estimates

The sources of error in C_D are due to errors in measured tension, errors in measured velocity and the errors in measured strain. The following two figures provide estimates of the one standard deviation error bounds on the estimated C_D values. The greatest error occurs in the upper half of the pipe where the VIV response was smallest and the velocities were lowest.

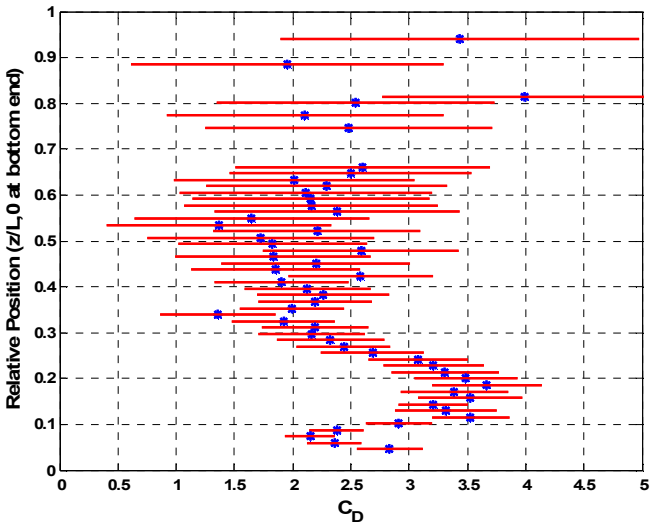

Figure 16. Error bounds on CD estimates for case 20061023205043. The blue dots show the mean value and the red line show the one standard deviation band on either side of the mean value.

Figure 16 shows the results for local C_D for case 20061023205043. The red lines indicate $C_D \pm 1$ standard deviation of the error. The details of the calculation of error are shown in [5].

The large error bands towards the top of the pipe show the uncertainty in the calculated C_D in this region. This region corresponds to low flow velocity (due to large incidence angles) and small values of static bending strains (Figure 10). It is best to neglect the results in this region (z/L=0.4 to z/L=1.0)

Figure 17 shows the results for local C_D for case 20061022153003. Again, the red lines indicate $C_D \pm 1$ standard deviation of the error. In this case, the error bands are larger because the noise in the strain measurements (estimated from the zero file) is very large. This results in the error bands being large over the entire length of the pipe and may result in an over prediction of the error. Even in this case, the error bands grow substantially in the region z/L=0.5 to z/L=1.0 and the drag values in this region should be ignored.

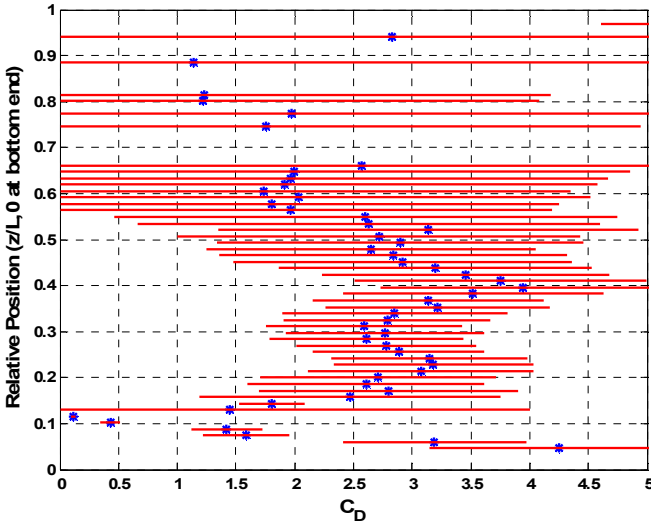

Figure 17. Error bounds on CD estimates for case 20061022153003. The blue dots show the mean value and the red line show the one standard deviation band on either side of the mean value.